Combined High-Resolution Active and Passive Imaging of Ocean Surface Winds from Aircraft

A.J. Gasiewski and J.R. Piepmeier
School of Electrical and Computer Engineering
Georgia Institute of Technology, Atlanta, GA 30332-0250
(404) 894-2934; (404) 894-2984
ag14@prism.gatech.edu; gt2930b@prism.gatech.edu

R.E. McIntosh, C.T. Swift, J.R. Carswell, W.J. Donnelly, and E. Knapp
Microwave Remote Sensing Laboratory
University of Massachusetts, Amherst, MA 01003
(413) 545-4858; FAX: (413) 545-4652
mcintosh@ecs.umass.edu; klemyk@ecs.umass.edu; carswell@alex.ecs.umass.edu; donnelly@alex.ecs.umass.edu; knapp@alex.ecs.umass.edu

E.R. Westwater, V.I. Irisov, and L.S. Fedor
NOAA Environmental Technology Laboratory, Boulder, CO 80303
(303) 497-6527; (303) 497-3577
ewestwater@etl.noaa.gov; virisov@etl.noaa.gov; lfedor@etl.noaa.gov

D.C. Vandemark
Laboratory for Hydrospheric Processes
NASA Goddard Space Flight Center, Wallops Island, VA 23337
(757) 824-2038; (757) 824-1036
vandemark@gsfc.nasa.gov

Abstract – A unique complement of passive and active microwave imaging and sensing instruments for observing ocean surface emission and scattering signatures were integrated onto the NASA Wallops Flight Facility's Orion P-3B aircraft (N426NA) for the purpose of studying the signature of ocean surface winds. The complement included: (i) a four-band (X, K, Ka, and W) tri-polarimetric scanning radiometer (PSR) (ii) a C-band ocean surface scatterometer (CSCAT), (iii) a Ka-band conical-scanning polarimetric radiometer (KASPR), (iv) a nadir-viewing Ka-band polarimetric radiometer, (KAPOL) (v) a 21- and 31-GHz zenith-viewing cloud and water vapor radiometer (CWVR), and (vi) a radar ocean wave spectrometer (ROWS). The above Ocean Winds Imaging (OWI) complement was flown during January-March, 1997 over the Labrador Sea. Conically-scanned brightness temperature and backscatter imagery were observed over open ocean for a variety of wind speeds and cloud conditions. Presented herein are the results of a preliminary intercomparison of data from several of the OWI instruments.

1. INTRODUCTION

Aircraft and satellite measurements have pointed to the possibility of building passive microwave sensors to measure both ocean surface wind speed and direction using the anisotropic nature of the emission from a wind-driven ocean. Such measurements would likely complement and improve upon wind vector maps available from active instruments (e.g., the NASA scatterometer - NSCAT). The need for complementarity is particular acute in high-wind conditions. Accordingly, the primary goal of the Ocean Winds Imaging (OWI) experiment was to collect data to verify the utility of passive polarimetric ocean wind vector sensing in high seas, with secondary goals being to better characterize the thermal emission and scattering signatures of a wind-driven ocean surface. The complement was flown under a variety of meteorological conditions in coordinated patterns over both ocean buoys along the eastern U.S. coast near Virginia and an instrumented research vessel - the *R.V. Knorr* - within the Labrador Sea. Local overflights of several NOAA ocean buoys near Wallops Island, VA and within the Gulf of Maine, and an extensive set of overflights of the Knorr located in the Labrador Sea during March 1-10, 1997 within the vicinity of 57°N, 53°W were performed. The conditions represented a wide range of surface wind speeds, cloud and water vapor states, and fetch lengths.

The OWI complement included two active radar scat-

terometers for measuring both Bragg and specular return (University of Massachusetts' C-band Scatterometer - CSCAT and the NASA/Wallops Flight Facility's Ku-band Radar Ocean Wave Spectrometer - ROWS), two passive polarimetric imaging radiometers for imaging the upwelling thermal emission from the ocean surface (Georgia Institute of Technology's Polarimetric Scanning Radiometer - PSR and the UMASS Ka-band Scanning Polarimetric Radiometer - KASPR), and precision fixed-beam radiometers for measuring the sub-track upwelling polarimetric emission from the ocean surface (the NOAA Environmental Technology Laboratory's Ka-band polarimetric radiometer - KAPOL) and the above-track thermal emission from clouds and water vapor (the NOAA/ETL Cloud and Water Vapor Radiometer - CWVR). The complement also included a GPS dropsonde package (provided by the National Center for Atmospheric Research) for measuring subtrack P,T,Q, and wind vector profiles, and several video cameras for recording ocean foam and cloud conditions. This paper provides a preliminary intercomparison of some scan-averaged data from the Labrador Sea deployment.

2. EXPERIMENT DESCRIPTION

Flight patterns used in the OWI experiment consisted primarily of straight and level transects forming "hex cross" patterns (Fig.1). The hex cross pattern allowed $\sim$ 30 km flight lines crossing the surface truth site at three different approach angles. Ship measurements included bulk meteorological quantities, ocean surface wind speed and direction, surface heat flux, long-wave directional spectra, and atmospheric profiles parameters via rawindsondes. Typical overflight altitudes were $\sim$ 5.5 km. A detailed description of the OWI sorties, including a discussion of the prevailing meteorological and sea conditions, the data observed by the various OWI sensors, the coincident data available from various sources, and the engineering and logistical issues encountered during the experiment, can be found in [1].

3. RADIOMETER OBSERVATIONS

The PSR consists of a gimbal-mounted scanhead drum containing four total power radiometers operating at 10.7, 18.7, 37, and 89 Ghz [2]. Each radiometer measures the first three modified Stokes' parameters ($T_v = \langle |E_v|^2 \rangle$, $T_h = \langle |E_h|^2 \rangle$, and $T_U = 2\Re\langle E_v E_h^* \rangle$). A two-axis stepper-motor drive system allows the radiometer scanhead to be positioned at arbitrary azimuth and elevation angles. External hot and ambient calibration loads are view once per scan to provide absolute radiometric calibration. Analog detection hardware is used to measure the orthogonal-polarized brightness temperatures T_v and T_h. A bank of three-level digital correlators operating at 1 GS/sec is used for the measurement of T_U and for redundant measurements of T_v and T_h.

Fig. 2 shows calibrated X-band vertical and horizontal brightness temperature variations observed during conical scans with a 53.1° incidence angle. Each plot is an average of several complete (360°) azimuthal scans observed during three hex-cross transects oriented in N-NE, W, and S-SE directions and flown on March 4, 1997 from 1502-1548 UTC. The brightness imagery have been corrected for roll and pitch variations using an empirical limb brightening function derived from a series of cross-track scans that were performed during banked turns. The radiometric noise was reduced by averaging to $\sim$ 0.8 K for each of $\sim$ 280 azimuthal points.

The plots show a distinctive 3-5 K up-wind/downwind anisotropy with second harmonic dependence with consistent phases between transects. The wind was reported by the Knorr to be from 270° at 15 m/secs with gusts to 18 m/sec, 4.8 m swell from 275°. It is seen that the second harmonic content of the horizontal channels is significantly greater than that of the vertical channels. A similar harmonic distribution has been observed in both SSM/I data [3] and in simulations using an asymmetric wave geometrical optics (AWGO) model [4].

The 37-GHz KAPOL instrument was oriented in a nadir-staring configuration. A ferrimagnetic switch facilitated the observation of three linear polarizations (along track at 0°, and ±45° from along-track) from which the first three Stokes parameters were computed according to $T_I = T_{45} + T_{-45}$, $T_Q = 2T_0 - T_{45} + T_{-45}$, and $T_U = T_{45} - T_{-45}$. The sensitivity of the KAPOL radiometer was $\sim$ 0.03 K for 1 second integration time.

At nadir, any polarization signatures (as seen in the second and the third Stokes parameters) can originate only from ocean surface anistropies. Such signatures can be seen in the KAPOL data observed during the three crossing transects of the hex cross. Fig. 3 shows a time record of T_I illustrating strong variations ($\gtrsim$ 10 K) due to the presence of the clouds between the aircraft and the sea surface. In contrast, T_Q and T_U show that noise due to clouds is mostly absent. Four strong variations in T_Q and T_U are related to rolls encountered during aircraft's turns. The absence of cloud signatures in T_Q and T_U is a result of the non-polarized nature of the phase matrix for electrically small cloud particles.

It is noted, however, that the mean levels of T_Q and T_U change in between aircraft turns as a result of changes in the polarization basis of the instrument. Such baseline data can thus be used to determine the apparent direction of the wind by estimating the predominant direction of the

polarization anisotropy. Fig. 4 shows recovered vectors of the brightness anisotropy along the hex-cross flight tracks obtained using a two-parameter (amplitude and phase) second harmonic fit to T_Q and T_U values. In these calculations, the KAPOL data was averaged over 30 seconds, and a 180^o directional ambiguity was resolved using in-situ wind measurements from the aircraft ($\sim 280^o$). The estimates compare well with reported surface winds measured by the Knorr and with the average surface winds measured using four GPS dropsondes released by the P-3 along a flight line in the vicinity of the hex-cross ($280^o \pm 15^o$ at 17 ± 1.5 m/sec).

The zenith-looking 21 and 31 GHz CWVR was similarly used to observe the impact of cloud emission reflected in the upwelling polarimetric ocean signatures. By flying beneath a broken cumulus cloud base on January 27, 1997, it was observed that warm perturbations of 3-4 K in the CWVR channels caused by clouds were strongly correlated with warm perturbations in the upwelling T_I as measured by KAPOL. However, the measurements of T_Q and T_U were virtually unaffected by the clouds.

4. RADAR OBSERVATIONS

The CSCAT radar [5] provided 360^o azimuthal scans of normalized radar cross-section simultaneously at incidence angles of 21^o, 31^o, 41.5^o, and 52^o. An example of an NRCS scan along with CMOD4 model fits is shown in Fig. 5 for the four incidence angles. Wind speed and direction estimates using CMOD4 curve fitting [6] during the period from 1447 to 1642 UTC resulted in consistent estimates of wind speed (15.5 m/sec average value) and direction (Fig. 6) for all four incidence angles. These wind speed and direction estimates are similarly in excellent agreement with the available surface truth.

ROWS data for the period from 1600-1642 UTC were similarly constant. Estimated sea surface parameters using the ROWS data [7] indicate a wind speed at 10 meters height $U_{10} = 13.34 \pm 0.95$ m/s, in reasonable agreement with both Knorr, dropsonde, and CSCAT observations. The ROWS data also indicate a significant wave height of 4.66 ± 0.31 m and RMS slope (at Ku-band) of 0.0438 ± 0.0024, consistent with high well-developed seas. These additional surface statistics are presently unavailable from the above active and passive instruments. ROWS will also be providing directional swell estimates for evaluating long-wave impact on the passive measurements.

5. SUMMARY

The above preliminary intercomparisons support the notion that active and passive remote sensing instruments can both be used to estimate wind direction. Indeed, excellent self-consistency among the variety of passive, active and contact sensors in both wind speed and direction was observed during the OWI experiment. Further intercomparisons are being made to determine the specific limitations of passive wind vector sensors in space. To expand the range of wind conditions for which data is available, additional deployments of the OWI complement of instruments are being planned in conjunction with instrument development studies in support of the NASA's EOS and the National Polar-Orbitting Operational Environmental Satellite System (NPOESS).

ACKNOWLEDGMENTS

The authors would like to thank R. Davidson, J. Baloun, and M. Tucker of the Raytheon Corporation for the design and fabrication of critical aircraft components; P. Bradfield, G. Postell, and the pilots and crew of N426NA for their outstanding help during the field campaign; and Drs. M. Van Woert of the U.S. Office of Naval Research, B. Douglas of the NASA/Headquarters Physical Oceanography Program, and S. Mango of the NPOESS Integrated Program Office for their support. GT acknowledges support from ONR grant NOOO14-96-1-0716, NPOESS IPO contract SMC 185-96-N0109, and NASA grant NAGW 4191; UMASS acknowledges support from ONR grants N00014-96-1-0698 and N00014-95-1-1034; NOAA/ETL acknowledges partial support from NOAA/NESDIS under contract MIPR-FY7615-96-NO243.

REFERENCES

[1] A.J. Gasiewski, J.R. Piepmeier, R.C. Lum, M. Klein, D. DeBoer, E.R. Westwater, V. Irisov, L. Fedor, C.T. Swift, R.A. McIntosh, J. Carswell, W.J. Donnelly, E. Knapp, and D. Vandemark, "Ocean Winds Imaging (OWI) experiment final report on NASA/WFF Orion P-3 integration and Labrador Sea field measurements", Tech. Rep., Georgia Institute of Technology, May 1997.

[2] J. R. Piepmeier and A. J. Gasiewski, "Polarimetric scanning radiometer for airborne microwave imaging studies", in *Proc. 1996 Int. Geosci. and Remote Sens. Symp. (IGARSS)*, University of Nebraska, Lincoln, NE, 1996, pp. 1688–1691.

[3] F. J. Wentz, "Measurement of oceanic wind vector using satellite microwave radiometers", *IEEE Trans. Geosci. Remote Sens.*, vol. 30, no. 5, pp. 960–972, September 1992.

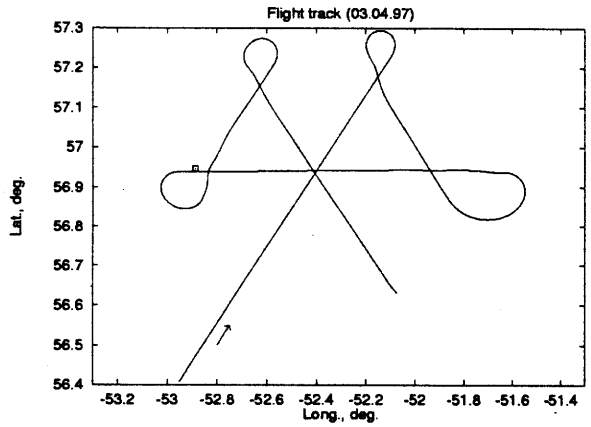

Figure 1: Hex-cross flight pattern used during OWI/Labrador Sea observations of ocean-surface anisotropies on March 4, 1997.

[4] D. B. Kunkee and A. J. Gasiewski, "Simulation of passive microwave wind-direction signatures over the ocean using an asymmetric wave geometrical optics model", *Radio Science*, vol. 32, no. 1, pp. 59–78, January-February 1997.

[5] J. R. Carswell, R. E. McIntosh, S. C. Carson, F. K. Li, G. Neumann, D. J. McLaughlin, J. C. Wilkerson, and P. G. Black, "Airborne scatterometers: Investigating ocean backscatter under low- and high-wind conditions", *Proceedings of the IEEE*, vol. 82, no. 12, pp. 1835–1860, 1994.

[6] European Space Agency, "CMOD4 model description", Electrosciences Report ER-TN-ESA-GP-1120, European Space Agency, 1993.

[7] D. Vandemark, F.C. Jackson, E.J. Walsh, and B. Chapron, "Airborne measurements of ocean wave spectra and wind speed during the Grand Banks ERS-1 SAR Wave Experiment", *Atmosphere-Ocean*, vol. 32, no. 1, pp. 143–178, 1994.

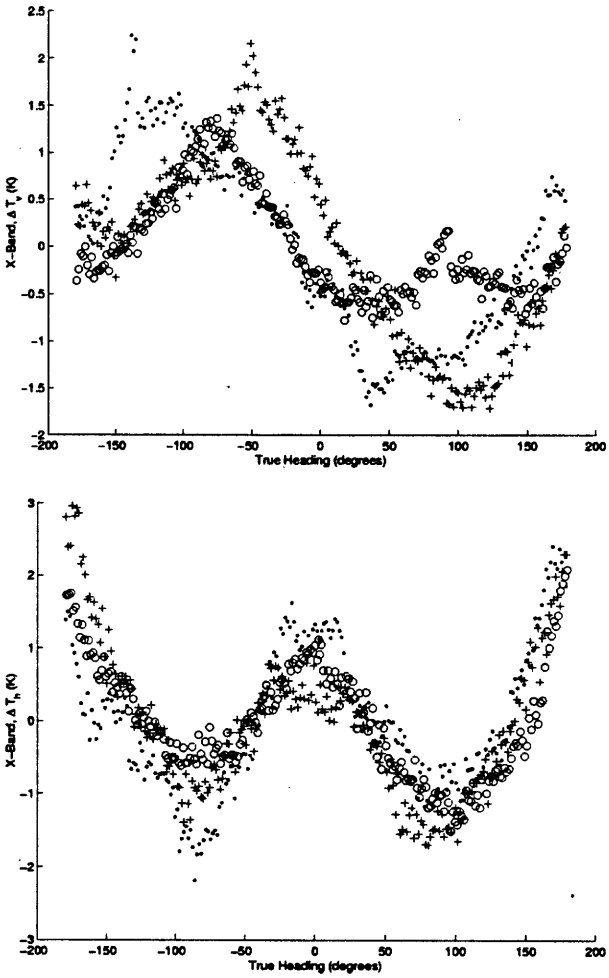

Figure 2: Calibrated PSR X-band azimuthal scans for a series of straight transects referenced to true north.

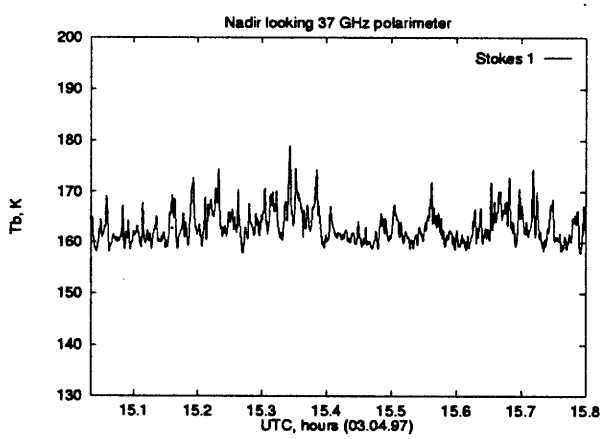

Figure 3: First Stokes parameter as observed using KAPOL during three transects of the hex-cross pattern in Fig. 1.

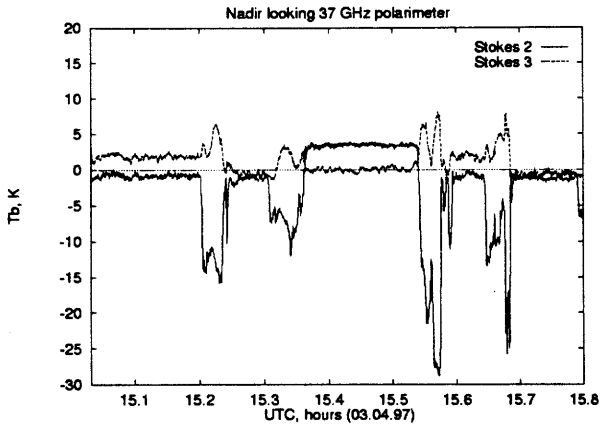

Figure 4: Second and third Stokes parameters as observed using KAPOL during three transects of the hex-cross pattern in Fig. 1.

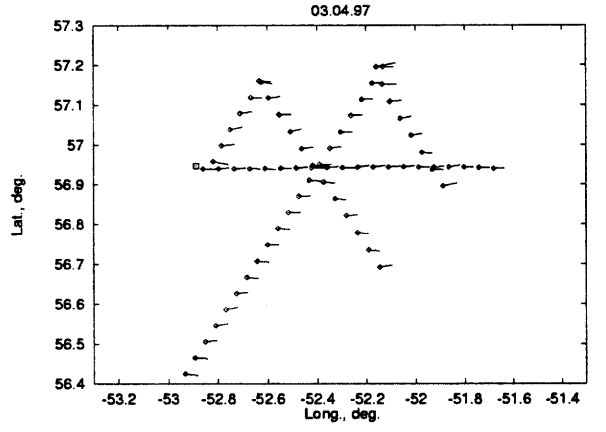

Figure 5: Ocean surface wind anisotropy vector determined from KAPOL data.

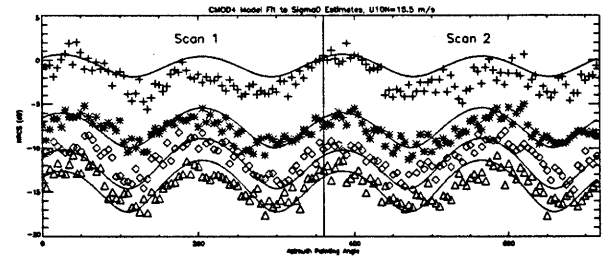

Figure 6: Azimuthal scans of normalized radar cross section observed at four incident angles using CSCAT.

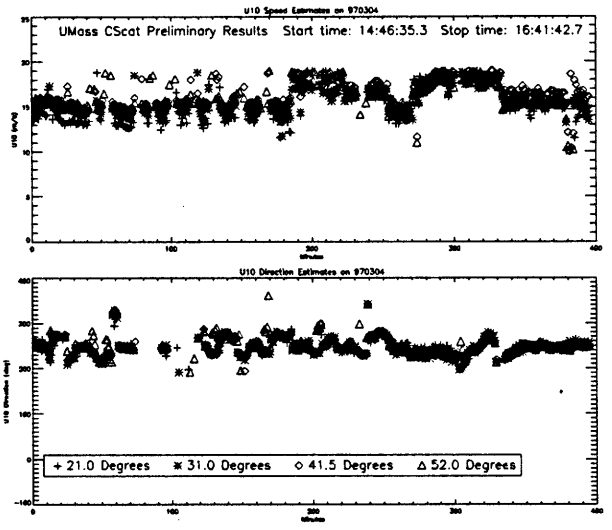

Figure 7: Estimated wind speed and direction using CSCAT data and the CMOD4 inversion model.